Pure & Appl. Chem., Vol. 60, No. 5, pp. 781–794, 1988.
Printed in Great Britain.
© 1988 IUPAC

Ionized cluster beam (ICB) deposition and processes

T.Takagi

Ion Beam Engineering Experimental Laboratory
Kyoto University Sakyo, Kyoto 606, Japan

Abstract - Ionized cluster beam (ICB) deposition is an ion-assisted film deposition technique by which high quality films of metals, dielectric and semiconductor can be formed at a low substrate temperature. In the ICB process, film materials are vaporized from a confinement crucible under conditions which result in the formation of aggregates of atoms (clusters). Clusters are ionized by electron impact and subsequently accelerated by high potentials. Through selection of available parameters, it is possible to control the average energy of depositing species over the range from thermal to above 200 eV per atom, which make possible well controlled crystalline film deposition and epitaxy. In the ICB deposition, characteristics of the deposition are mainly caused by both the structural characteristic of the clusters and the effect of ionization and acceleration of the clusters. Unique features of ICB deposition, reactive-ICB deposition and simultaneous deposition by use of ICB and microwave ion source are described with respect to the kinetic energy and the ionic charge by comparing those of deposition methods in plasma.

INTRODUCTION

About 15 years have passed since the ionized cluster beam (ICB) technique was initiated in our laboratory (ref. 1). The major target to be addressed initially was the development of a new fabrication technology to produce high quality thin films for functional devices at high deposition rates by utilizing the effects of ion bombardment and the influence of the charge of ionized particles. Since then, cluster formation has been studied theoretically as well as experimentally. Various kinds of thin film materials have also been deposited including semiconductors, metals, dielectrics for electronic devices, optical coatings, opto-electronic devices, magnetic, thermoelectric, and organic materials (ref. 2).

The special features of the ICB technology can be summarized as follows:
(1) Large macroaggregates (clusters) consisting of 100 to 2000 atoms are generated by pure vapor expansion, though it has been regarded as difficult to form such clusters from materials that are in the solid state at room temperature.
(2) The clusters, whose constituent atoms are loosely coupled together, are ionized and transported to substrates together with neutral clusters. By this means, we have established an ion transportation technique that can produce extremely low energy ion beams of the order of several eV to several hundreds eV with equivalently high intensity, and which is suitable for film deposition.
(3) When the clusters bombard a depositing surface, adatom migration can be enhanced by increasing the acceleration voltage. This is useful for making high quality film at low substrate temperature.
(4) A new technology for film formation and crystal growth has been developed by making effective use of the interaction of the substrate with impinging ionized and neutral clusters and the effects of ions in the film formation. The effect of ionic charge of the cluster is sufficient to influence film formation, even when the number of the electric charges in the total flux is extremely few. Since ICB is characterized by very small charge-to-mass ratio, deposition on semiconductors and insulators become possible without charging problems.

ICB studies have been made with respect to both cluster formation and thin film formation. Fundamental studies of large size cluster formation by using condensation theory have shown clearly the ICB operating conditions. Through these studies, an important ambiguity in the treatment of metal cluster formation by the classical condensation theory could be addressed. There were several important factors in the theoretical discussion of the cluster formation by supersaturation of adiabatically expanding vaporized solid materials which have essentially large surface tension. The first was the energy barrier height for cluster formation, the second was the nucleation rate of critical nuclei, and the last was the growth

rate for large clusters. By an analysis based upon σ/T (ref. 3), that is the surface tension σ divided by the operation temperature T, it was revealed that vaporized solid materials have even lower nucleation energy barrier height and higher nucleation rate than gaseous materials. A computer simulation also indicated that the vaporized solid materials have higher efficiency for cluster growth (ref. 4). Recent emphasis in the cluster formation study has been placed on the direct observation of clusters collected on a liquid nitrogen temperature substrate. Several types of ICB equipments are now commercially available in Japan and in the United States (ref. 5).

By ICB bombardment experiment, it has been clearly shown that the kinetic energy of the individual atoms in the accelerated clusters is much lower than those of single ions. In the low energy range which ICB can offer, we have already demonstrated explicitly the effects of acceleration voltage upon adatom migration, nucleation density, sticking coefficient and enhancement of chemical reactions (ref. 6). The charge of the ions has notable effects in enhancing film formation activity and chemical reaction, even without intensive acceleration of ions and even with small fractions of ions. These studies contributed to the understanding of the film formation mechanism by ICB.

By ICB deposition, many different thin films of metals, semiconductors, insulators, and organic materials have been deposited. They showed important characteristics which can apply thermally stable semiconductor metallization, very thin film multiple layer coating with suppressed inter-diffusion at high temperature, high quality semiconductor and insulator devices and organic electron devices (refs.2,5). Al epitaxy on Si and dielectric materials (ref. 7), all-single-crystalline $Al/CaF_2/Si$ systems (ref. 8), high quality and large area GaAs film epitaxy (ref. 9), CdTe/PbTe superlattice formation (ref. 10), high quality Al_2O_3 (ref. 11) and CaF_2 depositions on low temperature substrates (ref. 12), and controlled crystalline organic film deposition (ref. 13) were highlights in the last two years.

This chapter describes present understanding of the cluster beam formation mechanism and the present status and ability of film deposition by standard ICB and reactive ICB (R-ICB) which is used under reactive gas atmosphere at relatively low pressure. Simultaneous deposition method by a microwave ion source and an ICB source has been used for oxide or nitride deposition. This current modification of ICB deposition is unique because of the high reactivity of oxygen or nitrogen. This process helps to bring about low temperature film deposition.

CLUSTER FORMATION PROCESS

From the standpoint of material sciences, clusters and their research areas could be classified as shown in Figure 1 (ref. 14). One area concerns the region of small clusters with less than several tens of atoms. The other region is that of the ultra-fine particles with a size of some 10^4 atoms or more (ref. 15). In the former, chemical approach has been made to investigate cluster properties. Many researchers have been engaged in this region. In the study of the ultra-fine particles, the physical approach has prevailed so far.

The unique feature of the cluster formation in the ICB method is that the source material is in solid state at room temperature. The clusters are generated by ejecting the vaporized source material from a confinement type crucible into high vacuum region as a supersonic nozzle beam. The classical nucleation theory, or liquid droplet theory, deals with a cluster as a liquid droplet and gives the Gibbs free energy G for a cluster of radius r in terms of the surface tension as follows.

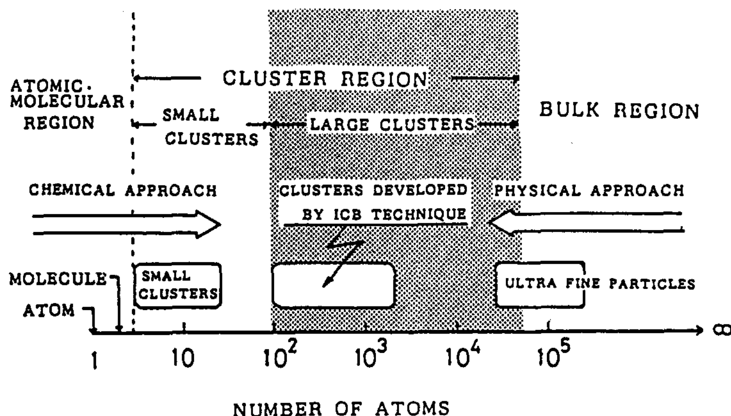

Fig. 1. Classification of cluster regimes from the standpoint of material science.

$$(\Delta G)_{max} = \Delta G^* = 16\pi\sigma^3/3(kT/v)^2(\ln S)^2, \quad (1)$$

where, v is the molecular volume in cluster, and S is the saturation ratio P/P_0, P_0 being the equilibrium vapor pressure. With an assumption of thermally stable equilibrium, the nucleation rate J of the clusters is expressed as

$$J = K \exp(-\Delta G^*/kT), \quad (2)$$

where, K is a factor which varies much slowly with P and T compared to the exponential term. Though several expressions for K have been developed so far, the most common equation was given by Frenkel (ref. 16) as

$$K = (P/kT)^2 v(2\sigma/\pi m)^{1/2}. \quad (3)$$

Equations (1) and (2) show that the energy barrier height for cluster formation is strongly influenced by the surface tension. Since σ is cubed in the exponent of eq. (2), J is largely dependent on it. Therefore, there has been a misunderstanding that it is hard to form clusters from metals (whose surface tensions are much larger than those of liquefied gases) by supersonic expansion. We have pointed out (ref. 3) that such a simple discussion is not correct since J is a function of $(\sigma/kT)^3$, instead of σ^3. Because the vaporization temperatures of metals are much higher than gaseous materials, comparison of σ does not give a correct discussion. Moreover, the surface tension of a cluster might differ significantly from the commonly referred flat plane value, because considerable portion of atoms in a cluster are situated on its surface and the physical properties of clusters are strongly affected by the surface atoms. For example, Tolman (ref. 17) reported that the cluster surface tension decreases with decreasing the cluster radius as

$$\sigma = \sigma_\infty/(1+2\delta/r), \quad (4)$$

where, δ is a correction factor of the order of the atomic radius. In this event, the clusters may be formed more easily than expected from a calculation using flat plane value of σ.

Figure 2 shows the $\Delta G/kT$ for several materials as a function of cluster radius r under the condition of P = 10 Torr and S = 100. It is seen that in spite of large surface tension, the free energy of formation of metals, with the exception of Hg, are not higher than those of gases. Figure 3 shows the cluster nucleation rate as a function of saturation ratio. Since the nucleation rate of 10^{20} - 10^{24} $/m^3$sec is considered to be a criterion for cluster formation, metal clusters are expected to be formed as easily as gas clusters.

COMPUTER SIMULATION OF CLUSTER FORMATION

By using the classical nucleation theory, the cluster formation process of Al and Ar has been simulated. The gasdynamical equations for conservation of mass, momentum, and energy are

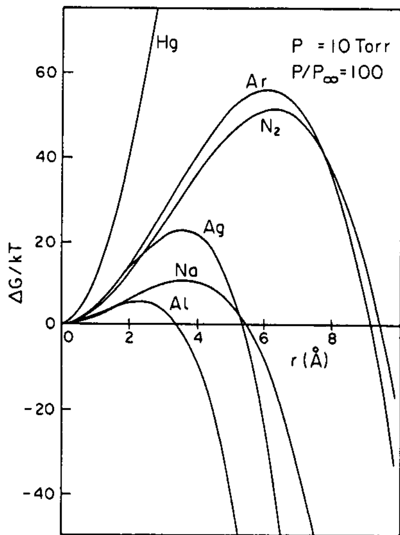

Fig. 2 $\Delta G/kT$ as a function of cluster radius for several materials at P=10 Torr and S=100.

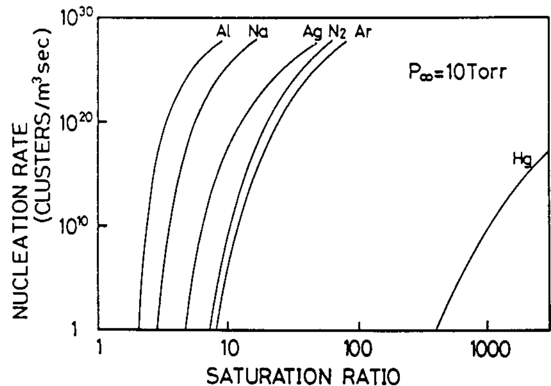

Fig. 3 Cluster nucleation rates for several materials as a function of saturation ratio at P=10 Torr.

expressed as

$$\frac{d}{dx}\frac{\rho A u}{1-\mu} = 0; \qquad (5)$$

$$u\frac{du}{dx} + \frac{1-\mu}{\rho}\frac{dP}{dx} = 0; \qquad (6)$$

$$u\frac{du}{dx} + (1-\mu)C_p\frac{dT}{dx} = h_{fg}\frac{d\mu}{dx}, \qquad (7)$$

where, ρ is the vapor density, A the cross sectional area of the flow, μ the mass ratio of condensed and vapor phase, and h_{fg} is the latent heat of condensation.

The vapor flow geometry, as shown in Fig. 4, was assumed as a function of distance x as follows.

$$A = (\pi D^2/4)[1 + (2x\tan(\theta/2)/D)^2], \qquad (8)$$

where, D, the throat diameter, is 2 mm and θ, the nozzle opening angle, was 30 degrees. Figure 5 shows the results of the variation of the relative vapor temperature T/T_0 and relative flow pressure P/P_0, for Al (a) and Ar (b), where T_0 and P_0 are respectively source (crucible) temperature and source pressure (vapor pressure in the crucible). The source condition was set to a saturated vapor and the flat plane surface tension was used for these calculations. An increase of P_0 over several Torr promotes the cluster formation, which can be seen from the increase in the relative flow temperature caused by the latent heat of condensation. It is seen that the condensation of Al vapor starts from the negative value of distance x, that is, upstream of the throat. On the other hand, cluster formation of Ar requires higher P_0 than that for Al.

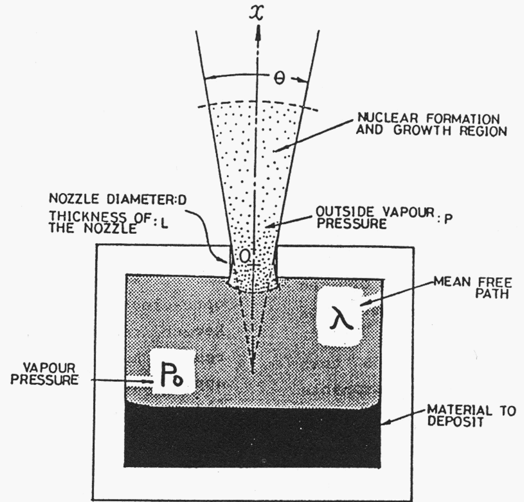

Fig. 4 ICB soruce parameters and flow geometry.

Figure 6 shows the simulation results of cluster size distribution for Al at a distance x = 6 mm from the throat. The lower side of the size distribution is attributed to those clusters that were formed at relatively large distances from nozzle throat, while the larger clusters represent those generated at an upstream region and continue to grow down stream.

The foregoing results are not qualitatively exact. Because it must be remembered that the classical nucleation theory used for the computations identifies the nucleation rate for a particular vapor state with the equilibrium concentration of clusters of critical size for that state. In addition, the calculation involves obscure physical parameters such as surface tension, density, and sticking coefficient for clusters. Notwithstanding the fact that the present nucleation theory does not give quantitatively reliable results for cluster formation in supersonic expansions, it can be utilized to compare on a qualitative basis the tendency for cluster formation of different gases. Our calculations imply that metal vapor is more likely to form clusters compared to gases under comparable expansion conditions.

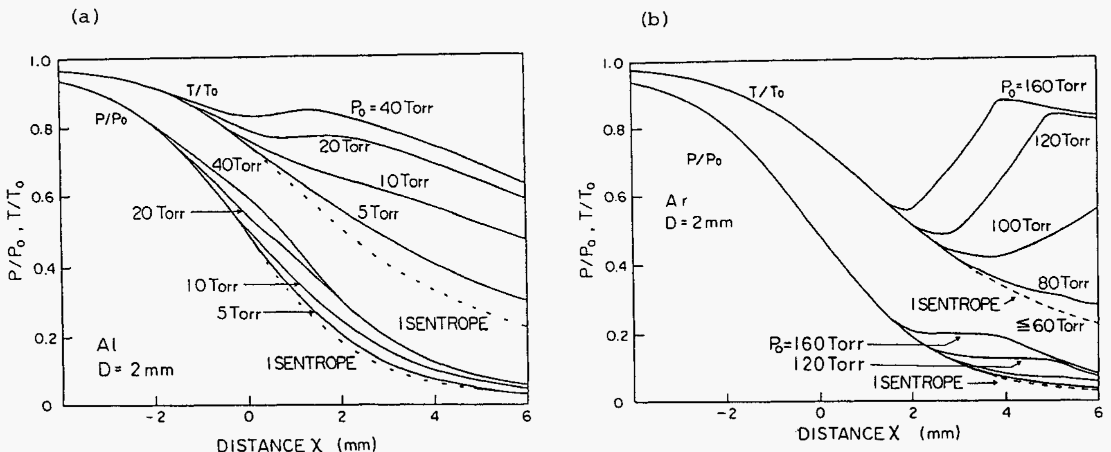

Fig. 5 Variations of relative flow temperature T/T_0 and pressure P/P_0 of cluster beam along the expansion for Al (a) and Ar (b).

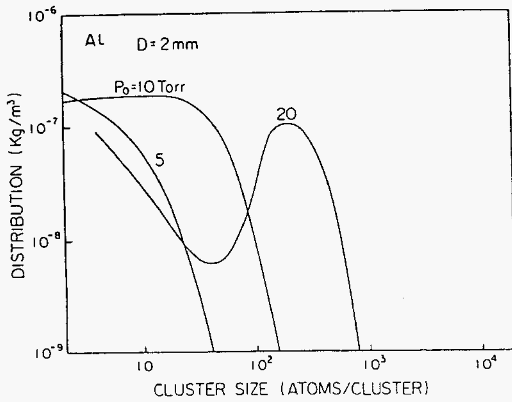

Fig. 6 Size distribution of Al clusters obtained by the simulation under different source pressures P_0.

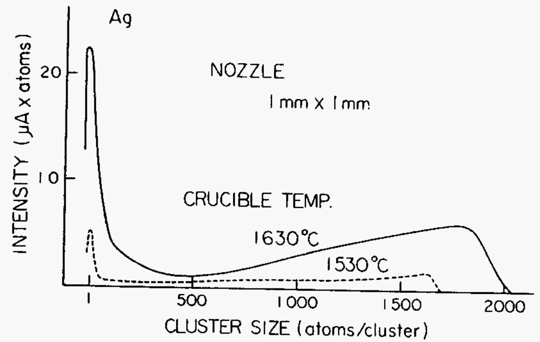

Fig. 7 Size distribution of Ag clusters measured by the retarding field method.

CLUSTER SIZE DISTRIBUTION

The most common experimental method for evaluating cluster size is energy analysis either by the retarding field method or by the electrostatic energy analyser. Since the kinetic energy of a cluster is proportional to its mass and velocity square, it is possible to estimate the cluster size by measuring the energy. Figure 7 shows an Ag cluster size distribution which ranges broadly from several hundreds to two thousand atoms/cluster. Beam intensity was increased by increasing the crucible temperature. The cluster size has also been evaluated by using an electrostatic energy analyser (ref. 18). The beam had energy in the range of 80-170 eV as a cluster. If the energy of each constituent atoms is assumed to be approximately 0.1-0.2 eV, the size of cluster will be 400-1700 atoms/cluster which is agreeing well with the results from the retarding field method and the TOF method. Those data show a similar size distribution, which means that the cluster is ionized in a singly charged state.

Transmission electron microscope (TEM) observation have also been made (ref. 19). The clusters were collected on carbon films which were cooled down to liquid nitrogen temperature. The deposition rate and collection time were chosen so as to avoid coalescence of the clusters on the substrate surface. Figure 8 shows a typical TEM image of Ag clusters for a crucible temperature of 1680 K and nozzle diameter of 1 mm. The deposition rate measured by QCO monitor was about 2 nm/min. For a deposition time shorter than 6 sec, the cluster size distribution showed no substantial variation, while the number density of the cluster increased linearly with the deposition time until 6 sec. It is considered that there is no coalescence for deposition time shorter than 6 sec. The mean cluster diameter under this condition was about 2 nm. Since there are some experimental results reporting that the clusters on the surface are stable at least at room temperature (ref. 20), the image shown in Figure 8 may be shown to be representation of clusters generated by the vapor ejection. Though the detailed information on the shape and density of clusters has not been investigated, the result of TEM observation suggests that the cluster size is of the order of several hundreds atoms.

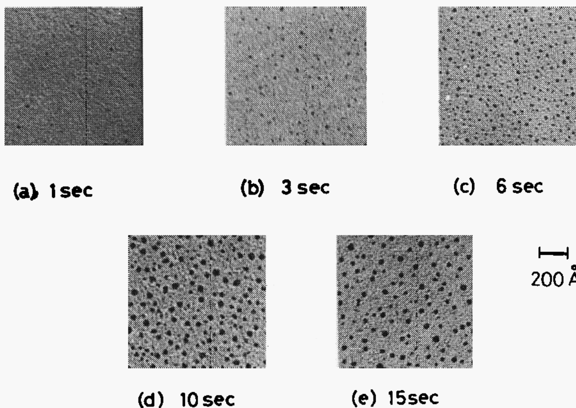

Fig. 8 TEM image of Ag clusters collected on a carbon film at liquid nitrogen temperature.

STRUCTURE OF CLUSTERS

Structures of vaporized metal clusters have been studied by electron diffraction of the cluster beam. A vaporized-metal cluster source was installed to the diffraction chamber of an electron microscope, and the cluster beam was crossed by a 45 keV electron beam (ref. 21). A diffraction pattern from a Sb cluster beam is shown in curve (B) of Figure 9 against the scattering parameter $s = 4\pi\sin(\theta/2)/\lambda$, where λ is the electron wavelength and θ is the scattered angle. A diffraction pattern of a polycrystalline Sb film is also shown in curve (C) for comparison. Debye rings indicating crystalline structure did not appear for cluster beam, but a halo pattern characteristic of amorphous structure was observed. This means that the vaporized metal clusters are quite different from microcrystallites and have no long-range ordering in the atomic arrangement. The radial distribution function obtained by Fourier transformation of this diffraction pattern indicated that the interatomic distance in the cluster is somewhat longer than those in Sb crystal or amorphous Sb film. Te and Bi cluster beams were also examined by electron diffraction. They both indicated similar halo patterns, suggesting that the vaporized-metal clusters produced by supersonic expansion of the pure vapor generally have amorphous structure. On the contrary, it is known that the microcrystalline metallic clusters, usually containing from several thousands to several tens of thousands atoms, can be generated by ejecting metals with inert carrier gas (ref. 22). The curve (A) in Figure 9 shows a diffraction pattern of Sb clusters generated with the expansion of Ar carrier gas of 1 Torr. The diffraction peaks line up but there is almost no significant difference from the microcrystalline diffraction pattern. This result partly reflects the fact that the clusters generated in the carrier gas is cooled down more efficiently than those in pure expansion because the carrier gas works as a heat sink, removing energy from clusters through molecular collisions. Another notable feature of the microcrystalline clusters is that the lattice parameter changes by reducing the cluster size. Moreover, in the case of In clusters, the crystal system changes from bulk f.c.-tetragonal structure to f.c.c. structure when the cluster size is decreased below 5 nm. Therefore, it is reasonable to conclude that the vaporized metal cluster formed by pure expansion consisting of around one thousand atoms have much different structure compared to those crystalline clusters, to say nothing of bulk crystals.

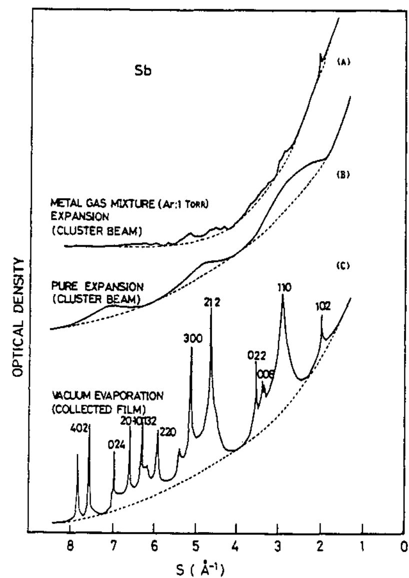

Fig. 9 Electron diffraction patterns of Sb cluster beams formed by (A) expansion of metal and gas (Ar, 1 Torr) mixture, and (B) expansion of pure Sb vapor. Diffraction pattern of a polycrystalline Sb film is also shown in (C).

KINETIC ENERGY RANGE OF IONIZED AND ACCELERATED CLUSTERS

The above mentioned properties of the vaporized-metal cluster beam have important correlation with the film formation process in the ICB deposition. Since the cluster has amorphous structure, the constituent atoms are considered to be loosely coupled to one another compared to those in the crystalline state. An ionized cluster accelerated at an appropriate acceleration voltage will break up on the substrate with the kinetic energy distributed evenly to individual atoms. The migration of the atoms on the substrates has an important role to enhance the film formation kinetics. Moreover, this process allows the production of equivalently low energy and high intensity ion beams without space charge problems.

Estimation of the surface disorder caused by ICB bombardment also gives an evidence of cluster formation. The surface crystallinity of Si substrates bombarded by Al cluster beams were measured by ion channeling after the Al film has been removed by chemical treatment (ref. 9). A Si substrate bombarded by 0.5 keV Ar ion beam to a dose of 2×10^{15} ions/cm^2 was also examined for comparison. Figure 10 shows the channeling spectra for 5 keV and 0.2 keV Al ICB bombarded surfaces, and the one by 0.5 keV Ar ion beam. Figure 11 shows the comparison of the surface damage by Ar ion bombardment. The result shows that the displacement of surface atoms induced by Al ICB bombardment is much smaller than that caused by the atomic Ar ion bombardment. Actually, the disorder caused by ICB bombardment is much smaller than that produced by naturally oxidized layer. It can be concluded that the kinetic energy of the individual atoms in an accelerated cluster as it impacts a surface appears no larger than the order of 10's of eV.

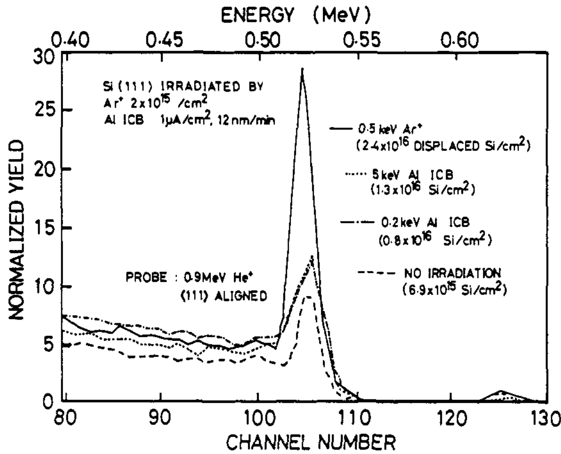

Fig. 10 He ion channeling spectra of Si substrate bombarded by Ar ion and Al cluster ion beams (Al has been etched off).

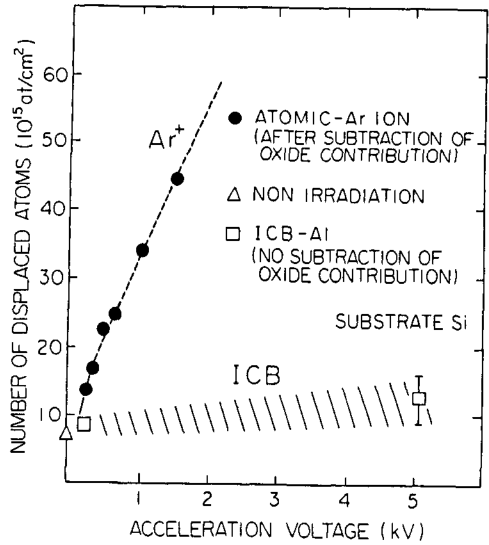

Fig. 11 Comparison of the numbers of displaced Si surface atoms produced by Ar ions and ICB-Al beams at different acceleration voltages.

ICB DEPOSITION EQUIPMENT

The basic ICB source is shown in Figure 12. In the ICB source in which clusters are created by condensation of supersaturated vapor atoms produced by an adiabatic expansion process, some clusters are ionized by electron impact. Kinetic energy can be added to the ionized clusters by applying an acceleration voltage. Commercial ICB equipment were recently introduced by several manufactures in Japan and already in the US. Basic configuration of the ICB sources is classified into a multi-nozzle type and a multi-crucible type. With multi-crucible system, simultaneous deposition and sequential deposition methods are possible. Figure 13 shows a photo of one of the commercially available systems (ref. 23). This equipment has multinozzles (5-25 nozzles) and the deposition rate reaches 1000 Å/min with Cu, Cr and Au. In Figure 14, construction of ICB chamber which can mount three ion sources is shown (ref. 24). The source produces a high flux density beam which can be used for semiconductor applications.

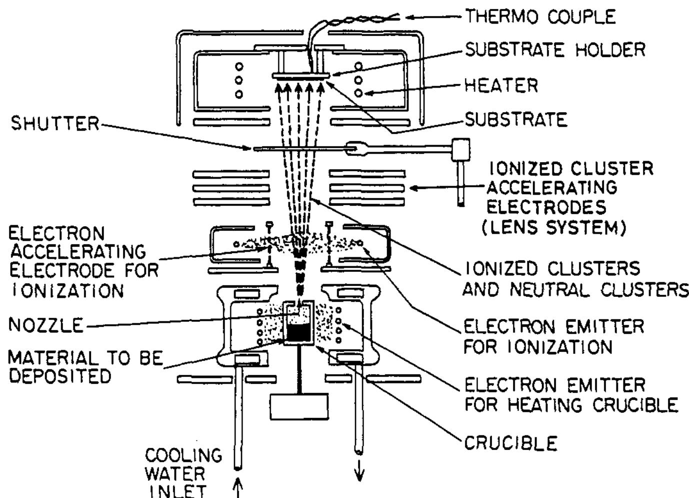

Fig. 12 Schematic diagram of a laboratory ICB system.

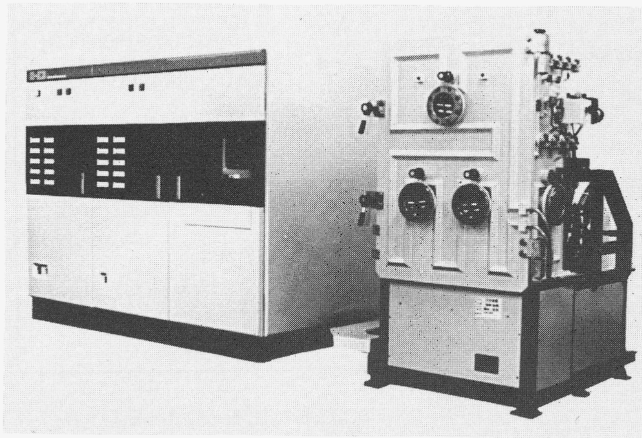

Fig. 13 Photo of ICB deposition system (Mitsubish M-ICB, D52 type).

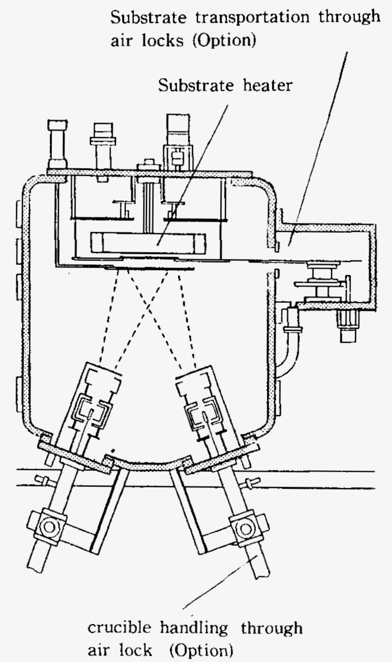

Fig. 14 Chamber construction of ICB system (Nissin ICB-2G type).

FILM FORMATION MECHANISMS

In ICB deposition, the following processes in the film formation are considered. When the clusters bombard the substrate surface, both ionized and neutral clusters are broken up into atoms which are then scattered over the surface with high surface diffusion energy. A scattered atom is physically attracted to the substrate surface but it may move over the surface (adatom migration) because of high momentum parallel to the surface derived from the incident kinetic energy. The adatom interacts with other adatoms and/or substrate atoms to form a stable nucleus and finally to cease its movement and become a chemically adsorbed atom. Thus, the enhanced adatom migration results in an increased nucleation rate and an increased growth rate of islands. But the adatoms which have not encountered other adatoms or nucleation sites also reevaporate with an increased rate. These process are shown in Figure 15.

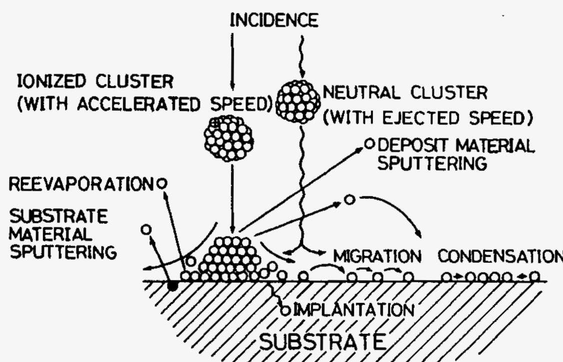

Fig. 15 Conceptional illustration of film formation by ICB.

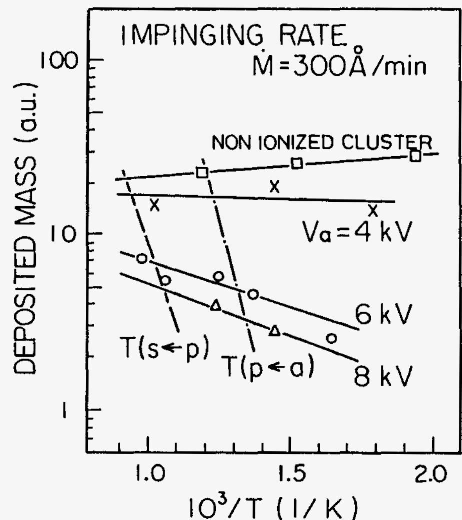

Fig. 16 Deposited mass versus reciprocal substrate temperature. T(s←p) and T(p←a) indicate polycrystalline to single crystal and amorphous to polycrystalline transition temperatures, respectively.

Unique effects of kinetic energy in film formation by ICB can be elucidated by measuring the deposited mass M on the substrate as a function of substrate temperature. The deposited mass M is expressed by (ref. 25).

$$M = \dot{M}t - (\dot{M}N_0/I^*)\exp(-U/kT), \qquad (9)$$

where $U = \phi_{ad} - \phi_d$, ϕ_{ad} is the activation energy for desorption and ϕ_d is the activation energy for surface diffusion, $\dot{M}$ is the mass impingement rate on the substrate, I^* is the rate of formation of critical nuclei, and N_0 is the density of adsorption sites on the substrate surface. Since ϕ_{ad} is generally larger than ϕ_d, the curve of mass versus the reciprocal of the temperature will have a positive slope. Figure 16 shows the mass deposited versus the reciprocal of the substrate temperature. The crystalline states of the films deposited at different acceleration voltages are also shown. For the non-ionized clusters corresponding to conventional deposition methods, the mass deposited increases with decreasing substrate temperature. The mass deposited at a given substrate temperature decreases with increasing acceleration voltage because of sputtering and reevaporation, and the slope changes with acceleration voltage. The change of the slope from positive to negative sign with increasing acceleration voltage is considered to be due to the change in values of the parameters N_0, I^*, and U. This is one of the important features of the ICB deposition process which differentiates it from conventional deposition processes using atomic, neutral or ionized particles, where the energy U does not change (ref. 26).

Migration and surface cleaning effects can be clearly seen in actual film deposition by comparing the Si epitaxial growth in an ultra high vacuum (UHV) and normal high vacuum chambers. Figure 17 shows the diffraction patterns of the films deposited at different deposition conditions. In the epitaxial growth of Si on an atomically clean and well-ordered silicon surface in the UHV chamber, only 200 V acceleration was enough to obtain epitaxial films at a substrate temperature (Ts) of 500 °C. By increasing acceleration voltage, crystalline quality could be improved. In the other hand, for the deposition in a chamber which was evacuated by an oil diffusion pump to a base pressure of 10^{-7} - 10^{-6} Torr, 6 kV or higher acceleration voltage was needed for silicon epitaxial films to be obtained. An amorphous or polycrystalline structure was formed in a range of 0 - 4 kV. In this deposition no special cleaning except for chemical processing was used prior to the deposition. In this case, higher acceleration voltage is required in order to remove the native oxide and impinging residual gas atoms from the substrate surface during the deposition. From the Rutherford backscattering spectra using 185keV H^+ and SIMS analysis, it was found that the film prepared has no increase in oxygen at the interface between the deposit and the substrate.

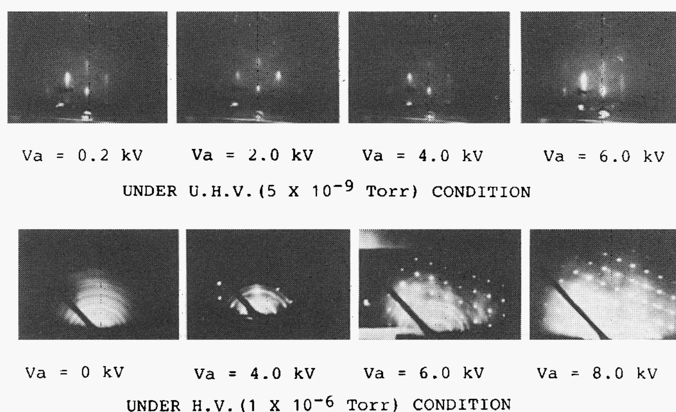

Fig. 17 Electron diffraction patterns of epitaxial silicon films by ICB at different acceleration voltages.

FILM DEPOSITION BY ICB

By ICB deposition, many different thin films of metals, semiconductors, insulators, and organic materials have been deposited. They showed important characteristics which can apply thermally stable semiconductor metallization, very thin film multiple-layer coating with suppressed inter-diffusion at high temperature, high quality semiconductor and insulator devices and organic electron devices (refs. 2,5). Here, a few areas of recent important examples of ICB deposition are described (ref. 27).

Metallization and interconnect technologies are important key factors gating further advancement in VLSI technology. Aluminium is widely used for contact electrodes and interconnects in silicon semiconductor devices. It is, however, important to establish the qualitative limits of the Al/Si system imposed by such problems as electromigration, hillock growth, alloy penetration, and interface stability. We have shown there limits and further extension of device performance by using ICB-Al films. In the formation of preferentially

oriented films on SiO_2 substrate, the degree of orientation increases monotonically by increasing the acceleration voltages. On Si(111) and Si(100) substrates, epitaxial Al films could be deposited. ICB deposited Al films on Si substrate were annealed for 30 min in the 450 -550 °C temperature range. No hillocs and valleys, as normally observed in the Al films prepared by conventional vacuum deposition could be seen. Also no degradation of the film crystallinity was observed. Auger electron spectroscopy measurement showed that the interface remained abrupt even after annealing at 550 °C. An electro-migration test showed that there was no change in resistance after 400 h of operation opposed to sputterd Al films that normally fail after 20 h.

Interface thermal stability of Cu-Al bilayer system has been studied. When accelerating ionized Cu and Al clusters, the bilayer films formed on Si substrate did not show any intermetallic compound formation even after annealing in a vacuum at 230 °C for 60 min. Only a small interdiffusion between Cu, Al and Si atoms was observed. Thus, thermally stable surfaces and interfaces in the bilayer films could be obtained with the aid of kinetic energy and ionic charge of cluster ions.

Study of thin multilayers films in the 1-10 nm range has become very important in both fundamental physics and advanced device application. CdTe-PbTe multilayerd structures (1.5 nm layer) have been constructed on InSb substrate at 250 °C by a dual ICB source using CdTe and PbTe ingots as source materials. The existence of an n=1 miniband in the potential well structure of 60 period films with a layer thickness of 6.5 and 8 nm respectively was also confirmed by optical absorption spectra.

Some GaAs thin films with high crystalline quality were recently prepared. Compared with MBE, ICB could be more suitable for industrial production because of much higher allowable deposition rates for crystal growth, and the possibilities of using a much larger substrate area, lower substrate temperature and more versatile doping methods. The films were deposited on (100) LEC GaAs substrates using dual Ga and As cluster beams, both partially ionized and accelerated to the substrate which was held at 500 - 600 °C under a background pressure of only 10^{-6} Torr. It is expected that the sticking coefficient of ICB deposited Ga is enhanced and less arsenic flux is required compared to that used in MBE. Reflection high energy electron diffraction (RHEED) patterns of the film deposited at an acceleration voltage of 1 kV showed a streaked pattern and Kikuchi lines, indicating surface smoothness in addition to the excellent crystallinity obtained. The RBS channelling spectra demonstrate that there is no measurable difference in the spectrum of the film compared to that of the substrate.

FILM DEPOSITION BY REACTIVE ICB DEPOSITION

By introducing reactive gas in the deposition chamber, formation of oxide, hydride or nitride films can be possible. The reactive gas pressure is in the order of 10^{-5} - 10^{-4} Torr. Some of reactive gas introduced into the chamber is ionized and dissociated in the ionization region of the ICB source. These species become active and contribute to enhancement of the reaction. Applying this condition, high quality a-Si:H, Al_2O_3, SiO_2, ZnO, BeO have been deposited at low substrate temperature (refs.28,29).

In a-Si:H deposition, thermally stable mono-hydrides have been obtained. In this deposition, silicon was deposited in a hydrogen ambient at 10^{-5} Torr. The hydrogen molecules in this pressure region do not collide significantly with silicon cluster beams. Therefore the chemical reaction occurred on the depositing surface. The reaction increased with the acceleration voltage. Figure 18 shows the relative numbers of particles impinging on the substrate surface. Since the background gas pressure before introducing the hydrogen gas was $5x10^{-7}$ Torr, the main particles impinging on the substrate surface are ionized and neutral silicon clusters from the ion source, and the mixed hydrogen gas and doping gases that are introduced into the chamber through the leak valves. The constituent parts of these gases are atomic and molecular hydrogen and their ions, because some of the hydrogen molecules are ionized and some are dissociated inside the ionizing section. Under typical deposition conditions, the number of impinging silicon atoms was in the order of 10^{15} - 10^{16} atoms/cm^2sec as calculated from the measured silicon ion-current density under the assumption that the average size of the cluster was 1000 atoms per cluster and that 10% of the total beam flux was ionized. The impinging rate of hydrogen ions was calculated to be 10^{13} ions/cm^2sec from the ion current to the substrate. The ratio of the hydrogen atoms to the hydrogen molecules was estimated from the change of H and H_2 peaks in a mass spectrum when the electrical input power into the source was varied. A 10 % increase in hydrogen atoms was observed when the input power was increased above the typical deposition condition. Since the rate of impinging hydrogen molecules is on the order of 10^{16} molecules/cm^2sec under operating conditions approximately 10^{15} atoms/cm^2sec of dissociated hydrogen atoms impinge on the substrate surface. Thus the rate of impinging hydrogen ions is three orders of magnitude smaller than that of molecular hydrogen. It is not clear yet which state of hydrogen is dominantly involved in the hydrogenation process. But it seems natural to consider that hydrogen ions could have a considerable influence in providing uniform

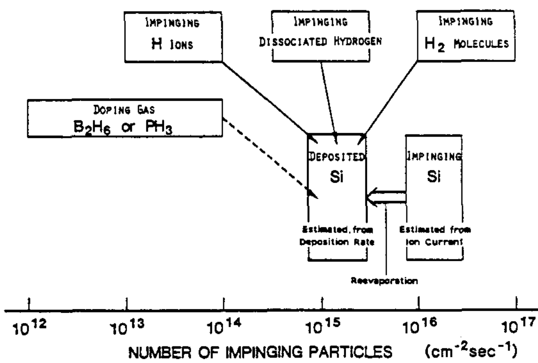

Fig. 18 Kinds of particles impinging on the substrate surface and estimated number of impinging particles.

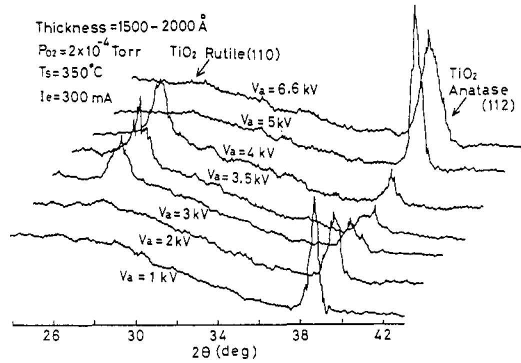

Fig. 19 X-ray diffractometer traces of TiO_2 films deposited at the acceleration voltages indicated.

hydrogenation. For doped film formation, hydrogen gas mixed with phosphine or diborane on the order of 5000 ppm was available sequentially in the same chamber. No problems arose as a result of the residual reactive gas used in previous processes. P- or n- type films could be reproducibly formed at practical deposition rates. The structural analysis showed that the film mainly consisted of monohydrides. The density of monohydrides can be increased by depositing at a higher acceleration voltage. In the RICB deposition of oxide, a gas pressure of less than 10^{-5} - 10^{-4} Torr was also sufficient to include chemical reactions without generating a plasma.

In TiO_2 deposition by R-ICB, the crystal phase of the films could be controlled by the content of ionized clusters and the acceleration voltage (ref. 30). The oxygen was introduced into the chamber in a range of 10^{-5} - 10^{-4} Torr. Ti was used as the source material. Figure 19 shows the change of crystalline structure examined by the X-ray diffractometer. The phase transition from anatase structure to rutile structure can be seen by increasing the acceleration voltage. The change of the structure occurred also by changing the ionization current.

Nitride films can also be formed in a nitrogen atmosphere in the pressure range of 10^{-5} - 10^{-4} Torr. GaN films with a hexagonal structure were formed by R-ICB. In this experiment, a ZnO film which was formed on a glass substrate by R-ICB was used as a intermediate layer to serve an adequate nucleation seed for growing a GaN film. The film was formed at the substrate temperature of 450 °C. Strong diffraction peak of the (002) plane was obtained (ref.31).

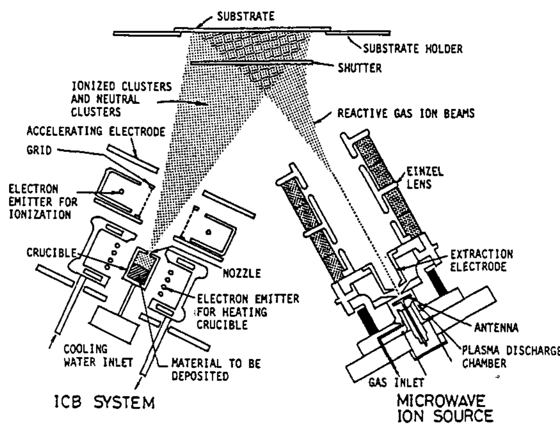

Fig. 20 Schematic diagram of the simultaneous use of a microwave ion source and an ICB system.

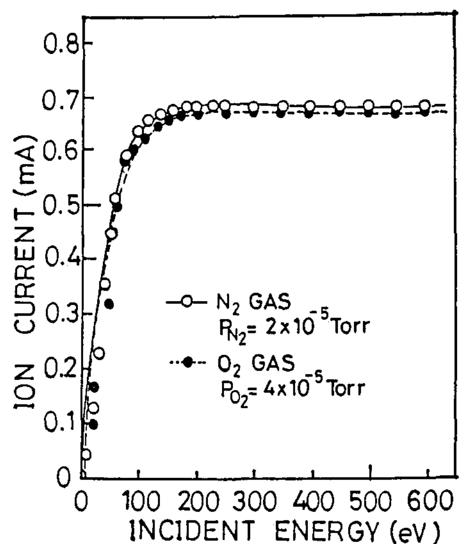

Fig. 21 Substrate ion current for N_2 and O_2 ions at different incident energy.

FILM DEPOSITION BY SIMULTANEOUS USE OF ICB AND MICROWAVE ION SOURCES

A new deposition technique by a simultaneous use of an ion source and deposition has already been proposed in 1973 (ref.32). As one of the modifications a simultaneous use of a microwave ion source and an ICB source has been developed. This technique has advantage, because the reactive gas ion energy and the current can be controlled independently from the ICB source operation. Therefore, the reactivities of the gases can be enhanced by selecting these operation conditions.

Figure 20 shows a schematic diagram of the simultaneous system of microwave ion source and ICB source. The detail of the microwave ion source is described elsewhere (ref. 33). The microwave source has a permanent magnet around the discharge chamber. The source operation can be set at the ECR condition which produces high density plasma. The gas ions are extracted by the extraction electrode applied at V_{ex}=3-15 kV and then the extracted ions are decelerated by the retarding filed produced between the source and the substrate holder down to 500 eV. Figure 21 shows the incident energy dependence of ion current measured at the substrate for the cases of N_2 and O_2 gas ions. The ion current increases with increasing the incident energy, and is saturated at about 100 eV.

AlN films have been deposited. The deposition conditions are listed in Table 1. High purity Al metal and N_2 gas were used as source materials. Sapphire (0001) and p-Si (111) were used as substrates. The substrate temperature (Ts) was at 100°C. Figure 22 shows the transmittance of the films prepared at different deposition conditions. In the case of neutral N_2 gas operation, the films were Al metallic colour and show no-transmittance as

TABLE 1 Deposition conditions for AlN films.

Al CLUSTERS (ICB)	
Evaporation Source	Al(99.9999%)
Crucible Temperature	1520°C (0.8Torr)
Electron Current for Ionization(Ie)	0mA(NEUTRAL) 200mA
Electron Energy for Ionization	300eV
Acceleration Voltage(Va)	0.5～2kV
N_2 GAS (Microwave Ion Source)	
Gas Source	N_2 (99.999%)
N_2 Gas Pressure in Chamber(P_{N_2})	2×10^{-6}Torr
Extraction Voltage	10kV
Nitrogen Ion Incident Energy	100～500eV

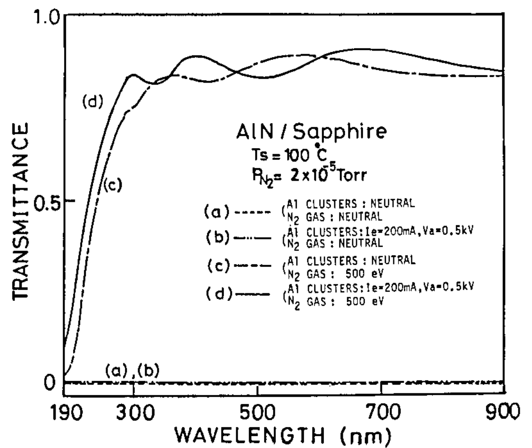

Fig. 22 Transmittances of the AlN films prepared at different deposition conditions for Al-Clusters and N_2 gas.

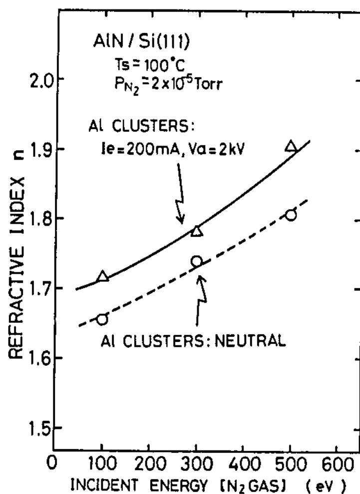

Fig. 23 Dependence of the refractive index of the AlN films on the incident energy for N_2 ions.

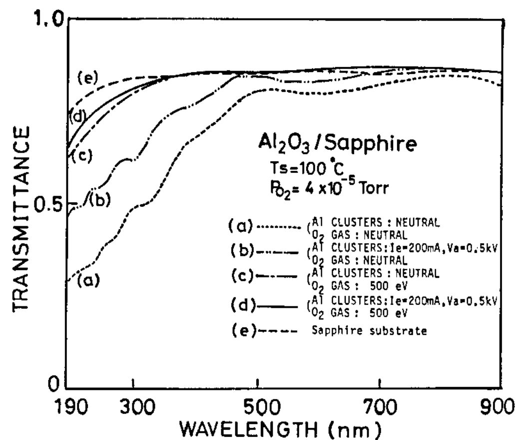

Fig. 24 Transmittances of the Al_2O_3 films prepared at different deposition conditions for Al-clusters and O_2 gas.

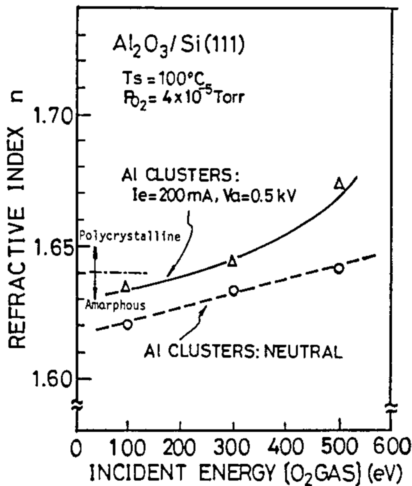

Fig. 25 Dependence of the refractive index of the Al_2O_3 films on the incident energy for O_2 ions.

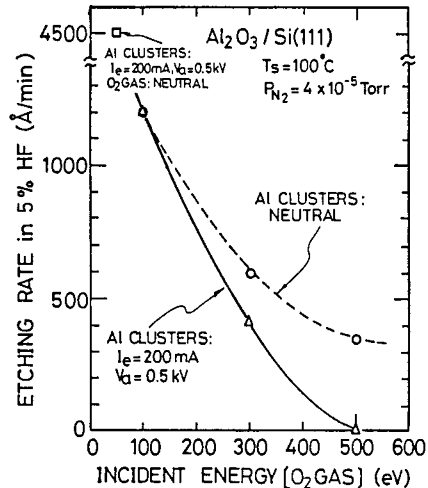

Fig. 26 Dependence of the etching rate for Al_2O_3 films on the incident energy for O_2 ions.

shown in (a) and (b) of the figure. However, in the case of N_2 ions with or without ionizing Al-clusters, the films deposited were transparent. The transmittances of the films were very large (see(c) and (d) in Figure 21). For these films, the composition ratio of N to Al was unity. Stoichiometric AlN films were confirmed by Rutherford Backscattering Spectroscopy (RBS). The obtained film was amorphous and chemically stable up to 1000°C.

Figure 23 shows the relationship between the incident energy of N_2 ions and the refractive index of the films deposited on Si(111) substrate. The refractive index (n) was measured by ellipsometry at the HeNe laser wavelength. As shown in the figure the refractive index is found to increase with increasing incident energy of N_2 ions. Also by using both N_2 ions and Al-ICB, the refractive index is larger than that of films deposited at the same incident energy by ionizing only N_2 gas.

As an example of oxide film formation, Al_2O_3 films have been deposited. Figure 24 shows the transmittance of the films prepared at different deposition conditions. In the case of using neutral Al-clusters and O_2 gas, the transmittance of the film is low, as shown in (a) of the figure. On the other hand, the films deposited with neutral Al clusters and O_2 ions became transparent, and the transmittances of the films increase. Also, in the case of the film deposited with both O_2 ions and ionized Al-clusters, the film was transparent and its transmittance was similar to that of the sapphire substrate used. It was found from RBS measurements that the composition ratio of oxygen to Al in these films was 0.67, and that stoichiometric Al_2O_3 films were formed. The film prepared at an incident energy of 500 eV for O_2 ions and an acceleration voltage of 0.5 kV for Al clusters was found to be thermally stable even after annealing at 1000 °C. Figure 25 shows the relationship between the incident energy of O_2 ions and the refractive index of the films deposited on Si(111) substrate. As shown in the figure, the refractive index (n) is found to increase with increasing the incident energy. Also, by using both O_2 ions and ionized Al-clusters, the refractive index is larger than that of the films deposited at the same incident energy by ionizing only O_2 ions. Figure 26 shows etching characteristics. 5% HF was used to etch the film. The etching rate is found to decrease with increasing incident energy, and in particular, in the case of using both O_2 ions and ionized Al-clusters, the film prepared at an incident energy of 500 eV is not etched. This fact indicates that the higher incident energy such as 500 eV increases the packing density of the film and the bonding between Al and O is considered to be effectively enhanced.

CONCLUSIONS

The ICB technique allows growth of not only single element or compound material films, but also hydrides, oxide and nitride films. The formation mechanism of the cluster beam, the fundamental film formation mechanism and some examples of the film properties have been shown. The films with well controlled crystallinity, even new material, can be deposited at a lower substrate temperature than those produced by other deposition methods by utilizing kinetic energy and ionic charge of ICB. Vacuum in the chamber during the deposition of these films was in the range of HV and UHV. In the case of RICB deposition, the residual gas pressure is approximately in the range of 10^{-5} - 10^{-4} Torr. Simultaneous use of ICB and microwave ion source for RICB has opened new applications for high quality oxide and nitride films deposited at lower substrate temperatures.

REFERENCES

1. T.Takagi, I.Yamada, M.Kunori and S.Kobiyama, Proc. 2nd Int. Conf. Ion Sources, 790-795, Österreichische Studiengesellshaft für Atomenergie, Vienna (1972).
2. T.Takagi, Vacuum 36, 27-31 (1986).
3. I.Yamada, Proc. Int. Ion Eng. Conf. -ISIAT'83 & IPAT'83- (Kyoto, 1983) 1177 - 1192, Inst. Elect. Eng. Japan, Tokyo (1983).
4. I.Yamada, H.Usui, and T.Takagi, Z. Phys. D. -Atoms, Molecules and Clusters 3, 137-142 (1986) and J. Phys. Chem. 91, 2463-2468 (1987)
5. T.Takagi, ed. Proc. Int. Workshop on Ionized Cluster Beam Technique, (Tokyo and Kyoto, 1986) Res. Group of Ion Eng., Kyoto Univ., Japan (1986).
6. T.Takagi, J. Vac. Sci. Technol. A2, 382-388 (1984).
7. I.Yamada, H.Inokawa, and T.Takagi, J. Appl. Phys. 56, 2746-2750 (1984).
8. I.Yamada, H.Takaoka, H.Usui, and T.Takagi, J. Vac. Sci. Technol. A4, 722-727 (1986).
9. I.Yamada, T.Takagi, P.R.Younger and J.Blake, SPIE Vol. 530, Advanced Applications of Ion Implantation, 75-83, Int. Soc. Opt. Eng., Washington (1985).
10. T.Takagi, H.Takaoka, Y.Kuriyama, and K.Matsubara, Thin Solid Films 126, 149-154 (1985).
11. H.Hashimoto, L.L. Levenson, H.Usui, I.Yamada and T.Takagi, Submitted to J. Appl. Phys.
12. I.Yamada, L.L. Levenson, H.Usui, and T.Takagi, (in press) 1987 MRS Spring Meeting Symposium Proceedings.
13. H.Usui, I.Yamada and T.Takagi, J. Vac. Sci. Technol. A4, 52-60 (1986).
14. T.Takagi, Oyo-Butsuri 55, 746-763 (1986).
15. F.Trager and G. Putlitz ed. Metal Clusters, Springer-Verlag, Heidelberg (1986).
16. J.Frenkel, Kinetic Theory of Liquids, Dover Publication, New York, 1955.
17. R.C.Tolman, J. Chem. Phys. 17, 333 (1949).
18. I.Yamada and T.Takagi, Thin Solid Films 80, 105-115 (1981).
19. I.Yamada and T.Takagi, Thin Solid Films 92, 137-146 (1982).
20. J.J.Metois, K.Heinemann, and H.Poppa, Appl. Phys. Lett. 29, 134-136 (1976).
21. I.Yamada, G.D.Stein, H.Usui and T.Takagi, Proc. 6th Symp. Ion Sources and Ion-Assisted Technol., 47-52, Inst. Elect. Eng. Japan, Tokyo (1982).
22. A.Yokozeki and G.D.Stein, J. Appl. Phys. 49, 2225-2232 (1978).
23. Technical data (Mitsubishi Co. Kitaitami, Hyogo, Japan.)
24. Technical data (Nissin Electric Co. Ukyo, Kyoto, Japan.)
25. C.A. Neugebauer in Handbook of Thin Film Technology, L.I. Maissel and R.Glang (eds.), McGraw-Hill, 8-15 (1970).
26. J.J.Metois, M.Gauch, A.Masson and R.Kern, Surf. Sci. 30, 43 (1972).
27. T.Takagi ed., Proc. 11th Symp. on Ion Sources and Ion-Assisted Technology -ISIAT'87-, Res. Group of Ion Eng., Kyoto Univ., Kyoto (1987).
28. T.Takagi, Emergent Process methods for high-technology ceramics, 425-446, ed. R.F. Davis, H.Palmour and R.L. Porter, Plenum Press, New York and London (1984).
29. T.Takagi in Semiconductor Technologies, 205-223, ed. J.Nishizawa, North-Holland, Amsterdam and Ohm, Tokyo (1984).
30. K.Fukushima, I.Yamada and T.Takagi, J. Appl. Phys. 58, 4146-4149 (1985).
31. K.Matsubara, T.Horibe, H.Takaoka and T.Takagi, Proc. 4th Symp. on Ion Sources and Ion Assisted Technology -ISIAT'80-, 137-140, Inst. Elect. Eng. of Japan (1980).
32. T.Takagi, I.Yamada and A.Sasaki, IEEE Trans ED-20, 1110-1114 (1973) and in Ion Implantation in Semiconductors, 275-283, Plenum Press, New York (1974).
33. J.Ishikawa, Y.Takeiri and T.Takagi, Rev. Sci. Instrum. 55, 449-456 (1984).